PHYSICAL REVIEW B VOLUME 43, NUMBER 10 1 APRIL 1991

Theory of electron-stimulated desorption of physisorbed species through a strongly bonding excited state

Zbigniew W. Gortel and Andrzej Wierzbicki
Department of Physics and Theoretical Physics Institute, Advadh Bhatia Physics Laboratory, University of Alberta, Edmonton, Alberta, Canada T6G 2J1
(Received 28 September 1990)

A model of the electron-stimulated desorption of physisorbed species is proposed in which the excited-state surface potential is due to a chemical rather than image force acting on the adsorbed particle after the initial electron excitation is completed. The equilibrium positions of the excited- and the ground-state potentials nearly coincide and desorption is a purely quantum-mechanical effect. A one-dimensional model is systematically derived from the three-dimensional theory. The oscillatory structure of the resulting kinetic-energy distributions of the desorbing species is predicted in certain cases. It is demonstrated that, unlike in the commonly accepted Antoniewicz model, both the kinetic-energy distributions of the desorbing neutral particles and the total desorption yield calculated in the present model are consistent with the experimental data for Ar and N_2O physisorbed on Ru(001).

I. INTRODUCTION

Photon- or electron-stimulated desorption (PSD or ESD, respectively) belongs to a wide class of processes in which the desorption is induced by electronic transitions (DIET).[1] In particular, photons or electrons can cause desorption by promoting a solid-adsorbate system to such a localized metastable electronic state, which decays by converting the electronic energy into nuclear motion. Other related processes of this kind include surface rearrangement, fragmentation,[2] and chemical reactions induced by electronic transitions. In laboratory practice one must account for DIET in any experiment involving the impact of energetic particles on solid surfaces, e.g., for surface diagnostic purposes. Studies of DIET are interesting also in their own right: Monitoring the desorption products (their kinetic energy, angular distributions, and state of internal excitations) one can gain insight into the initial binding states and into the dynamics of the relevant chemical processes.

Detailed microscopic mechanisms of desorption vary depending on the adsorbate-solid system involved. According to the commonly accepted view, the desorption process is a temporal sequence of a few independent processes (steps): (i) Initially, the system (electrons and atomic particles) is promoted by an external probe to a metastable electronic state with the excitation energy localized in the vicinity of the adsorbed particle. Creation of this initial excited state may be a quite complicated multistep process completed within some 10^{-16}s. (ii) Actual atomic positions of the adsorbed species may no longer be those for which the energy of all electrons is the lowest. Therefore, displacement of adsorbed particles occurs lasting some 10^{-14} to 10^{-13} s during which a slow adiabatic energy flow from electrons to adatoms takes place. The latter gain a substantial amount of kinetic energy provided a lifetime of the excited state is sufficiently long. (iii) If the initial electronic excitation weakens the adsorbed particle-surface bond, then the atomic displacement and the related increase of the kinetic energy of the adatom may lead to its desorption directly [Menzel-Gomer-Redhead (MGR) scenario of desorption].[3,4] It is also possible that the initial excitation strengthens the bond with the surface. In such a case a finite lifetime of the excited state is, in fact, a necessary condition for desorption. The kinetic energy gained during step (ii) is used to break the surface bond. A well-known example is the Antoniewicz scenario of desorption for physisorbed species.[5] (iv) Finally, the species escaping from the surface may still be modified and if this happens, then the analysis of the desorption process based on the properties of the desorption products becomes a very delicate problem.[6]

The interactions and the excitations involved in ESD of physisorbed atoms are expected to be the simplest to describe theoretically. Experimentally, the physisorbed systems are the most difficult to deal with because of their small binding energy. However, some experimental results are now available[7–14] allowing one to test the existing theoretical models. In all these attempts the use is made, in one way or another, of various versions of the Antoniewicz model[5] in which the physisorbed particle is ionized in the process of the initial electronic excitation mentioned above. Created in this way, the ion experiences an image force which attracts it towards the surface. Consequently, the ion moves towards the substrate [step (ii) above] and its reneutralization probability increases due to the large density of occupied electronic states of the metal which leak out of it. Therefore, the particle will finally undergo a transition [step (iii)] back to the repulsive branch of the electronic ground-state potential curve without changing its kinetic energy gained during step (ii). Step (iv) follows, during which the particle moves towards the surface, bounces back, and moves

 ©1991 The American Physical Society

away from it. It then may desorb provided it gained [in step (ii)] enough kinetic energy to avoid retrapping in the ground-state potential.

The Antoniewicz process was theoretically studied by a few authors, either in purely classical,[5,9,11,15] fully quantum-mechanical,[16,17] or approximate quantum-mechanical[18,19] approaches. An attempt was also made[20] to use the same model to describe ESD from chemisorbed layers. A common problem with all these attempts is their difficulty in accounting simultaneously for the total desorption yield and for the average kinetic energy (or, more precisely, the kinetic-energy distribution) of desorbing neutral particles: Usually, fitting the shape of the distribution to the experimental ones leads to calculated total desorption yields that are too low. Such a difficulty occurs for *all* physical systems for which the experimental data exist: N_2O/Ru(001),[11,15,16,18,19,21] Ar/Ru(001),[14,17,19,21] and Kr/Ru(001).[14,19,21] An agreement between theoretical results and the experimental observations can only be improved by assuming physically unjustified very strong position dependence of the electronic deexcitation (neutralization of the ion) probability[9,15–19,21] or by assuming the binding energy of a physisorbed atom weaker than experimentally determined.[17] A detailed review is given in Ref. 21.

It becomes clear from the above that an alternative to the Antoniewicz model mechanisms of ESD of physisorbed atoms should be considered. One such possibility is suggested by Jennison *et al.*[22] Their cluster calculations for He adsorbed on Cu indicate that the image potential does not describe properly the adsorbed particle binding to the surface in the excited state of the system. Hybridization of the excited atomic orbital (like 2*s* in He) with the substrate allows it to be filled with a screening electron immediately (i.e., within 10^{-16} s) after the physisorbed atom is ionized. Therefore, the rare-gas atom is not bound to the substrate by a strong image force but rather by a chemical bond similar to that experienced by an alkali atom which follows the rare-gas atom in the periodic table. Jennison *et al.*[22] have shown that He with a 1*s* hole binds to a Cu atom in a manner almost identical to that of Li. The force experienced by He in the excited state is substantially weaker than the bare image force, the excited state surface potential is substantially narrower than the one in the ground-state configuration, and the equilibrium positions of both potential curves nearly coincide.[22] No calculations of the excited-state potential curves were performed for other physisorbed systems. This state is also inaccessible to direct experimental probes. However, one might speculate that in the metastable electronic state produced as a result of the initial excitation, the particle is, also for other systems, bound to the surface by a potential which, although narrower than the ground-state surface potential, has its equilibrium position only slightly closer to the surface. One might ask then whether the ESD yields and energy distributions calculated in such a model are consistent with the experimental observations. We will show in this work that this is indeed the case and hope that our findings will stimulate discussion on the mechanism by which physisorbed species are desorbed upon initial electronic excitations.

Before studying the implications of the above model, we must realize that the scenario of desorption described at the beginning of this section must be modified: In step (i) the system is promoted to the electronic configuration in which the atom is bound to the surface by a potential $V_d(\mathbf{r})$, which is deeper and narrower than the ground-state potential $V_0(\mathbf{r})$ but has nearly the same equilibrium position. During step (i) the wave packet of the atom adjusts its width and phase to the potential $V_d(\mathbf{r})$ but little or no atomic displacement occurs. Step (iii) must then involve some kind of intra-atomic Auger process in which the screening electron fills the electronic ground state of the atom and another electron is released into the continuum. Some degree of interatomic electronic transfer must occur because the atom should end up as neutral.

In contrast to all standard models of stimulated desorption, the atom almost does not change its position during the lifetime of the excited state and it acquires little or no classical momentum. Consequently, a fully classical model predicts that no desorption takes place and if it occurs nevertheless it must be a purely quantum effect. One might ask then whether any substantial desorption can be achieved at all considering the fact that the results of the quantum-mechanical and of the classical approach almost coincide[16] for the Antoniewicz model. Part of the answer follows. Consider the time-dependent wave packet representing a particle evolving on the excited-state potential-energy surface. At $t=0$ it is a minimum uncertainty wave packet and its time-dependent average kinetic energy can be written as

$$2m\langle E_{\rm kin}(t)\rangle=\langle p(t)\rangle^2+[\Delta p(t)]^2 . \tag{1.1}$$

The first contribution at the right-hand side varies in time according to classical mechanics, whereas the square of the momentum uncertainty represents a purely quantum-mechanical contribution. In the Antoniewicz model the initial wave packet of the adsorbed particle is placed on a steep section of the excited-state potential. Its width subsequently increases, at least during the initial stages of its time evolution. Therefore, $\Delta p(t)$ decreases or remains constant at best. The increase of the kinetic energy is achieved because the average momentum increases and this effect is well described by classical mechanics. Not surprisingly, quantum effects in the Antoniewicz model are rather small. In contrast, in the present model $\langle p(t)\rangle$ is insignificant but the width of the packet decreases because it is initially placed near a bottom of a very narrow potential surface. Consequently, the momentum uncertainty increases, leading to the necessary desorption increase of the average kinetic energy, and this effect can only be described by a quantum theory.

In the remainder of the paper, Sec. II is devoted to a detailed formulation of the theory. The general theoretical framework is presented in Sec. II A. Usually, a one-dimensional approach to ESD is used without any justification. We remedy this shortcoming in Sec. II B where the one-dimensional approach is justified and we show how the angular distributions of desorbing species

can be theoretically described in such an approach. The model is then specified in Sec. II C. Expressions for the desorption yield and the kinetic-energy distribution of the desorption products are derived there, adopting Morse potentials for both surface potentials, and Heller's method[23] is used to describe a time evolution of the adsorbed particle's wave packet. In Sec. II D some additional approximations are made, leading to simple expressions for the kinetic-energy distributions and desorption yields. General features of these results are also discussed there. Numerical results are presented in Sec. III. First, various types of kinetic-energy distributions which can be obtained from our model are presented and discussed in Sec. III A. Application to ESD of N_2O and Ar physisorbed on Ru(001) is done in Sec. III B. We demonstrate that, unlike the commonly accepted Antoniewicz model, both kinetic-energy distributions of desorbing neutral particles *and* the total desorption yields obtained in our model are consistent with the existing experimental data. A short summary of the present model and a preliminary discussion of its results for the above two systems were already reported.[24] A final discussion and summary follows in Sec. IV. Additional lengthy formulas and derivations are given in three Appendixes.

III. THEORY

A. General formulation

Full quantum-mechanical theory of ESD was formulated a few times in the past,[25–27] most recently in Ref. 16. In a nutshell, following the initial excitation caused by the electron beam, the adsorbed particle is placed at $t=0$ on the excited-state potential-energy surface $V_d(\mathbf{r})$. We denote by A and A^* the adsorbed particle in the electronic ground and the excited state of the entire system, respectively (the superscript $*$ suggests that the excitation should be localized in the vicinity of A). The initial wave packet of A^* is $\chi_d^0(\mathbf{r})$ and it is usually approximated by the ground-state wave function of A in the surface potential $V_0(\mathbf{r})$. The following time evolution of the wave packet $\chi_d(\mathbf{r},t)$ of A^* is controlled by the time-dependent Schrödinger equation which, in addition to $V_d(\mathbf{r})$, contains an imaginary optical potential $V_{\rm opt}(\mathbf{r})=-i\hbar\lambda(\mathbf{r})/2$, accounting for the electronic deexcitation processes (i.e., transitions from A^* to A) and acting as a drain on the probability amplitude of A^*. $\lambda(\mathbf{r})$ is a position-dependent deexcitation probability per unit time (deexcitation rate). The results of the standard Antoniewicz model are very sensitive[15,16] to the details of the position dependence of $\lambda(\mathbf{r})$ (which in this case is often referred to as the reneutralization rate). In the present model, in which the center of the wave packet $\chi_d(\mathbf{r},t)$ does not move by any substantial amount, we ignore this position dependence, setting $\lambda(\mathbf{r})=\lambda=$const. Consequently,

$$\chi_d(\mathbf{r},t)=\exp(-\lambda t/2)\psi(\mathbf{r},t)$$

with $\psi(\mathbf{r},t)$ satisfying a standard time-dependent Schrödinger equation,

$$\left[-\frac{\hbar^2}{2m}\nabla^2+V_d(\mathbf{r})\right]\psi(\mathbf{r},t)=i\hbar\frac{\partial}{\partial t}\psi(\mathbf{r},t)\ , \tag{2.1}$$

subjected to the initial condition $\psi(\mathbf{r},t=0)=\chi_d^0(\mathbf{r})$.

The quantity of immediate interest is the probability $P(\mathbf{q})$ that the particle A in its electronic ground state desorbs with momentum $\hbar\mathbf{q}$. If $\phi_{\mathbf{q}}(\mathbf{r})$ is the continuum-state eigenfunction of the Hamiltonian

$$H_0=(-\hbar^2/2m)\nabla^2+V_0(\mathbf{r})$$

corresponding to the eigenvalue $\mathcal{E}_{\mathbf{q}}$—the kinetic energy of the detected particle—then $P(\mathbf{q})$ is given by

$$P(\mathbf{q})=\lambda\int_0^\infty dt\, e^{-\lambda t}|\langle\phi_{\mathbf{q}}|\psi(t)\rangle|^2\ . \tag{2.2}$$

Similarly,

$$P_{\mathbf{n}}=\lambda\int_0^\infty dt\, e^{-\lambda t}|\langle\phi_{\mathbf{n}}|\psi(t)\rangle|^2 \tag{2.3}$$

is the probability that the particle A does not desorb but is merely retrapped in a particular eigenstate of H_0 localized near the surface (a particle in such an eigenstate belongs to the adsorbate). In Eq. (2.3), $\mathbf{n}$ denotes a set of quantum numbers needed to specify such a state; the corresponding eigenfunction and the energy eigenvalue are $\phi_{\mathbf{n}}(\mathbf{r})$ and $\mathcal{E}_{\mathbf{n}}$, respectively. Obviously, $\phi_{\mathbf{n}}$ and $\phi_{\mathbf{q}}$ form a complete set of states; therefore, the total desorption yield is equal to

$$Y=1-\sum_{\mathbf{n}}P_{\mathbf{n}}=\sum_{\mathbf{q}}P(\mathbf{q})\ . \tag{2.4}$$

For the isotropic surface $P(\mathbf{q})=P(Q,q)$, where $q=q_z$ and $Q=(q_x^2+q_y^2)^{1/2}$, and the z axis is normal to the surface pointing toward the gas phase. The number of particles detected per second within a unit solid angle in the direction (θ,ϕ) and having kinetic energy within the unit energy interval around E is given by

$$\frac{d\dot{N}(E,\theta)}{dE\,d\Omega}=\frac{1}{2}\left[\frac{LA}{4\pi^3}\right]\left[\frac{2m}{\hbar^2}\right]^{3/2}\times\sqrt{E}\,P[Q=(\sqrt{2mE}/\hbar)\sin\theta, q=(\sqrt{2mE}/\hbar)\cos\theta], \tag{2.5}$$

where L and A are, respectively, the length of the gas container along the z axis and the area of the container perpendicular to it.

B. Reduction to a one-dimensional theory

The main task is a calculation of $P(Q,q)$ and $P_{\mathbf{n}}$. It requires, first of all, a solution of the time-dependent Schrödinger equation (2.1) and of the stationary Schrödinger equation for the eigenfunctions of H_0 for both the gas and the adsorbed phase. With certain plausible assumptions about the surface potentials $V_0(\mathbf{r})$ and $V_d(\mathbf{r})$, the problem can be considerably simplified. Starting with the ground-state surface potential, we split it into the z-dependent average surface potential $V_0(z)$ and

the remainder $\Delta V_0(\mathbf{R},z)$ accounting for the surface corrugation:

$$V_0(\mathbf{R},z)=V_0(z)+\Delta V_0(\mathbf{R},z) .$$

As usually, $\mathbf{R}$ is a component of $\mathbf{r}$ along the surface. One can use the basis formed by the bound $[\phi_n(z)]$ and the continuum $[\phi_q(z)]$ state eigenfunctions of the one-dimensional Hamiltonian containing only the average potential $V_0(z)$ to expand the eigenfunctions $\phi(\mathbf{r})$ of the three-dimensional Hamiltonian containing full surface potential. For the localized adsorption one can assume in the lowest-order approximation that (i) the off-diagonal matrix elements of $\Delta V_0(\mathbf{R},z)$ in the above basis vanish, (ii) the particle in the gas phase does not experience any corrugation (i.e., $\langle\phi_q|\Delta V_0|\phi_q\rangle=0$), (iii) $\langle\phi_n|\Delta V_0|\phi_n\rangle$ does not depend on n, and (iv) tunneling of the adsorbed particle from one adsorption site to any other can be ignored. With all these approximations, the eigenfunctions $\phi(\mathbf{r})$ and the corresponding energy eigenvalues can be written as

$$\phi_{\mathbf{q}}(\mathbf{r})=A^{-1/2}e^{i\mathbf{Q}\cdot\mathbf{R}}\phi_q(z) ,$$
$$\mathcal{E}_{\mathbf{q}}=\hbar^2(Q^2+q^2)/2m , \tag{2.6}$$

for the particle in the gas phase with momentum $\hbar\mathbf{q}=\hbar(\mathbf{Q},q)$ and

$$\phi_{\mathbf{n}}(\mathbf{r})\equiv\phi_{n,m,l}(\mathbf{r})=a_m(\mathbf{R}-\mathbf{R}_l)\phi_n(z) ,$$
$$\mathcal{E}_{n,m}=\mathcal{E}_n+\mathcal{E}_m^L , \tag{2.7}$$

for the particle adsorbed at the adsorption site $\mathbf{R}_l$. The eigenvalue $\mathcal{E}_n$ corresponds to the one-dimensional eigenfunction $\phi_n(z)$, whereas $a_m(\mathbf{R})$ is a function which, owing to assumption (iv), is the solution of the two-dimensional Schrödinger equation

$$\left[-\frac{\hbar^2}{2m}\left[\frac{\partial^2}{\partial x^2}+\frac{\partial^2}{\partial y^2}\right]+V_0^L(\mathbf{R})\right]a_m(\mathbf{R})=\mathcal{E}_m^L a_m(\mathbf{R}) . \tag{2.8}$$

The potential $V_0^L(\mathbf{R})$ in Eq. (2.8) is defined by [cf. (iii) above]

$$\langle\phi_n|\nabla V_0|\phi_n\rangle=\sum_l V_0^L(\mathbf{R}-\mathbf{R}_l)$$

and the assumption is made that V_0^L has the same form for each adsorption site. Note that the eigenfunctions (2.6) for the particle in the gas phase are orthogonal to the eigenfunctions (2.7) of the adsorbed particle, and that the orthogonality holds within each set also. The approximations leading to the above solutions are equivalent to the assumption that the surface potential $V_0(\mathbf{R},z)$ can be written as

$$V_0(\mathbf{r})=V_0(z) \tag{2.9}$$

for the particle in the gas phase and as

$$V_0(\mathbf{r})=V_0(z)+V_0^L(\mathbf{R}) \tag{2.10}$$

for the particle adsorbed at the $\mathbf{R}_l=\mathbf{0}$ adsorption site.

Convenient analytical representations of the potentials in Eqs. (2.9) and (2.10) allowing for analytical solutions for $\phi_n(z)$, $\phi_q(z)$, and $a_m(\mathbf{R})$ are the Morse potential for the average surface potential $V_0(z)$ and the two-dimensional harmonic-oscillator potential for $V_0^L(\mathbf{R})$.

Turning our attention to the time-dependent Schrödinger equation (2.1), we observe first that, within the approximation in which the initial wave packet is just the ground state of H_0, it has the form (2.7)

$$\psi(\mathbf{r},t=0)\equiv\phi_0(\mathbf{r})=a_0(\mathbf{R})\phi_0(z) , \tag{2.11}$$

where the subscripts 0 denote the ground states in each of the potentials into which $V_0(\mathbf{r})$ is split in Eq. (2.10). If we assume that similar splitting is justified for the excited-state surface potential $V_d(\mathbf{r})=V_d(z)+V_d^L(\mathbf{R})$, then the time-dependent Schrödinger equation (2.1) yields two equations. The time evolution of the z-dependent factor of the wave packet is determined by

$$\left[-\frac{\hbar^2}{2m}\frac{\partial^2}{\partial z^2}+V_d(z)\right]\psi(z,t)=i\hbar\frac{\partial}{\partial t}\psi(z,t) , \tag{2.12}$$

with the initial condition $\psi(z,t=0)\equiv\phi_0(z)$. A similar, but two-dimensional equation determines the time evolution of the $\mathbf{R}$-dependent factor for which the initial wave function is $a_0(\mathbf{R})$. The latter equation can be solved analytically if the lateral potential $V_0^L(\mathbf{R})$ is approximated by the two-dimensional harmonic potential which, in general, can be different than $V_d^L(\mathbf{R})$. We will assume, however, that $V_0^L(\mathbf{R})=V_d^L(\mathbf{R})$ because (i) no information on corrugation (and on its dependence on electronic excitation) is available and (ii) this simplification affects only the angular distributions but not the kinetic-energy distribution of the desorption products in the forward direction. With this assumption the $\mathbf{R}$-dependent factor of the time-dependent wave packet $\psi(\mathbf{r},t)$ is stationary and the probability $P(\mathbf{q})$ given by Eq. (2.2) reduces to

$$P(\mathbf{q})=F(\mathbf{Q})P^{(1)}(q) , \tag{2.13}$$

where

$$F(\mathbf{Q})=\frac{1}{A}|\langle e^{i\mathbf{Q}\cdot\mathbf{R}}|a_0(\mathbf{R})\rangle|^2 \tag{2.14}$$

and

$$P^{(1)}(q)=\lambda\int_0^\infty dt\, e^{-\lambda t}|\langle\phi_q|\psi(t)\rangle|^2 \tag{2.15}$$

is the probability of detecting the particle with a momentum $\hbar q$ which would be obtained in the entirely one-dimensional theory: The matrix element in Eq. (2.15) is an integral of the wave functions which depend only on z. In addition, the lack of tunneling between adsorption sites allows one to define the one-dimensional retrapping probability P_n into one of the excited states of the one-dimensional surface potential $V_0(z)$. In analogy to Eq. (2.3), it reads

$$P_n^{(1)}=\lambda\int_0^\infty dt\, e^{-\lambda t}|\langle\phi_n|\psi(t)\rangle|^2 . \tag{2.16}$$

The two-dimensional plane waves form a complete set of functions in their own right; therefore, $\sum_{\mathbf{Q}}F(\mathbf{Q})=1$. In

addition, $\phi_q(z)$ and $\phi_n(z)$ also form the complete set of functions of z. Consequently, Eq. (2.4) for the total desorption yield reduces to

$$Y=1-\sum_n P_n^{(1)}=\sum_q P^{(1)}(q) , \tag{2.17}$$

indicating that it is entirely determined by the one-dimensional theory.

Turning our attention to the kinetic-energy distribution of desorbing particles, we note first that within the one-dimensional theory it is obtained from $P^{(1)}(q)$ by multiplying it by the one-dimensional density of states. One gets

$$\frac{d\dot{N}^{(1)}(E)}{dE}=\left[\frac{L}{2\pi}\right]\left[\frac{2m}{\hbar^2}\right]^{1/2}\frac{P^{(1)}(q=\sqrt{2mE}/\hbar)}{\sqrt{E}} . \tag{2.18}$$

Consequently, owing to the factorization (2.13) of $P(\mathbf{Q},q)$, the three-dimensional angular energy distribution (2.5) can be written as

$$\frac{d\dot{N}(E,\theta)}{dE\,d\Omega}=\frac{A}{4\pi^2}\left[\frac{2m}{\hbar^2}\right]F[Q=(\sqrt{2me}/\hbar)\sin\theta]\times\left[\frac{d\dot{N}^{(1)}(E')}{dE'}\right]_{E'=E\cos^2\theta}E\cos\theta , \tag{2.19}$$

where we have anticipated that $F(\mathbf{Q})=F(Q)$ for the isotropic ground-state wave function $a_0(\mathbf{R})$. Note the Knudsen-law factor $\cos\theta$ in Eq. (2.19). For desorption in the direction normal to the surface, one gets from Eq. (2.19) (after multiplying it by 2π to account for all azimuthal directions)

$$\frac{d\dot{N}(E)}{dE}=\left[\frac{A}{2\pi}\left[\frac{2m}{\hbar^2}\right]F(0)\right]E\frac{d\dot{N}^{(1)}(E)}{dE}=(4/\hbar\omega_L)E\frac{d\dot{N}(1)(E)}{dE} , \tag{2.20}$$

indicating that, within a constant factor, the kinetic-energy distribution is just the one-dimensional distribution multiplied by E. This result was anticipated in Refs. 15 and 16. The factor $4/\hbar\omega_L$ in Eq. (2.20) is obtained after taking for $a_0(\mathbf{R})$ the ground state of the two-dimensional isotropic harmonic potential with the angular frequency ω_L.

To summarize, we have been able to express the three-dimensional energy distributions in terms of the distributions usually obtained in the one-dimensional approach. The essential step was the ability to factorize $P(\mathbf{q})$ according to Eq. (2.13). There are essentially three approximations which make this factorization possible: (i) negligible tunneling in the adsorbate between adjacent adsorption sites (i.e., lack of band effects), (ii) negligible surface corrugation as seen by the particle moving away from the surface, and (iii) negligible dependence of the surface corrugation on the electronic excitation of the system $[V_0^L(\mathbf{R})\approx V_d^L(\mathbf{R})]$. Whereas approximations (i) and (ii) seem to be well justified for particles as heavy as Ar atoms, the approximation (iii) might be questionable. This approximation is, nonetheless, the easiest one to relax. There is no need to do this, however, as long as the distributions in the forward direction are of main concern.

C. Specification of the model

To proceed, we must specify the physical model we want to consider. In the standard Antoniewicz approach the potential $V_0(\mathbf{r})$ is the Van der Waals potential holding the physisorbed particle A near the surface. The incoming electron beam ionizes the adsorbed particle which, in the simplest approximation, is subsequently acted upon by the additional Coulomb image force. Thus, in the majority of works investigating ESD for physisorbed species,[9,11,15,16,18–21,28] the potential $V_d(\mathbf{r})$ is assumed to be a sum of the original potential $V_0(\mathbf{r})$ and of the Coulomb interaction potential of the ion A^* with its image. Forces somewhat weaker than those caused by the image interactions were also considered.[17] A common feature of all these approaches is the fact that the initial wave packet $\chi_d^0(\mathbf{r})$ of A^* is centered at a position much farther away from the surface than the equilibrium position of $V_d(\mathbf{r})$ and that the lifetime of A^* [determined by $V_{\rm opt}(\mathbf{r})$] is much shorter than the time A^* needs to travel to the inner turning point of $V_d(\mathbf{r})$. Therefore, the only important characteristic of $V_d(\mathbf{r})$ is its slope at the initial position of the wave packet. The classical theory is usually adequate to describe the process.[16,21]

As already discussed in the Introduction, the arguments were forwarded[22] that the image potential might not have anything to do with the process considered here because the lifetime of the ion created by the incoming electron beam is too short for any displacement of the ion to occur. Instead, the initial excitation is followed by an almost immediate electron relaxation leading to creation of the metastable excited electronic configuration in which A^* can be considered to be a chemisorbed particle experiencing a surface potential $V_d(\mathbf{r})$ which is much deeper and narrower than $V_0(\mathbf{r})$ but having its minimum almost at the same position as that of $V_0(\mathbf{r})$. Classical effects are negligible in this case and a quantum approach must be used to study it.

To calculate $P^{(1)}(q)$ given by Eq. (2.15), one needs the stationary continuum-spectrum wave functions $\phi_q(z)$ in the potential $V_0(z)$. These wave functions describe states in which the desorbing particles are detected. One also needs the solution $\psi(z,t)$ of the time-dependent Schrödinger equation (2.12). The initial wave packet for this equation is the ground-state wave function $\phi_0(z)$ in the potential $V_0(z)$. To solve the necessary Schrödinger equations, we must specify both one-dimensional potentials. We chose Morse potentials for both $V_0(z)$ and $V_d(z)$:

$$V_0(z)=V_0(e^{-2\gamma_0(z-z_0)}-2e^{-\gamma_0(z-z_0)}) , \tag{2.21a}$$

$$V_d(z)=V_d(e^{-2\gamma_d(z-z_d)}-2e^{-\gamma_d(z-z_d)}) . \tag{2.21b}$$

The analytical expressions for the eigenfunctions $\phi_n(z)$

and $\phi_q(z)$ are known and are listed in Appendix A. Also, the analytical form of the WKB approximation to $\phi_q(z)$ is given there. It is more useful for our purposes than the exact one (cf. Sec. II D).

Heller's method[23] is used to solve the time-dependent Schrödinger equation (2.12). One assumes that $\psi(z,t)$ has a form of Gaussian,

$$\psi(z,t)=\exp\left[\frac{i}{\hbar}\{\alpha(t)[z-z(t)]^2 +p(t)[z-z(t)]+\delta(t)\}\right], \quad (2.22)$$

where $\alpha(t)$ and $\delta(t)$ are in general complex. Expanding the potential $V_d(z)$ in a Taylor series around the instantaneous position $z(t)$ of the center of the wave packet, keeping only quadratic and lower-order terms in this expansion, and using the Schrödinger equation (2.12), one arrives at the set of ordinary differential equations for $z(t)$, $p(t)$, $\alpha(t)$, and $\delta(t)$. One usually assumes[23] that $z(t)$ and $p(t)$ represent just the classical motion that, for the Morse potential $V_d(z)$, can be obtained analytically. Im$[\delta(t)]$ is fixed by the overall normalization, Re$[\delta(t)]$ determines irrelevant overall phase factor, and the equation for $\alpha(t)$ is

$$\dot{\alpha}(t)=-\frac{2}{m}\alpha^2(t)-\tfrac{1}{2}V_d''(z(t)) . \quad (2.23)$$

For all potentials $V_d(z)$ for which analytical solution of the classical equations of motion for general initial conditions exist, Eq. (2.23) can be solved analytically. Details are given in Appendix B [Eq. (B5)]. The initial wave packet $\psi(z,t=0)$ is the ground-state wave function $\phi_0(z)$ in $V_0(z)$. In the method used here it must be replaced by the Gaussian (2.22) with $z(0)=z_0$, $p(0)=0$, and $\alpha(0)=\alpha_0=im\omega_0/2$, where $\omega_0=\gamma_0\sqrt{2V_0/m}$ is the angular frequency of oscillations at the bottom of $V_0(z)$. Both the exact analytical form of $\phi_0(z)$ and its Gaussian approximation are given in Eq. (B1).

In general, all wave functions needed can be expressed in terms of dimensionless functions of dimensionless positions ($\xi=\gamma_0 z$, $\xi_0=\gamma_0 z_0$), energy ($\varepsilon=\hbar^2q^2/2mV_0$), and time [$\tau=\omega_d t$, where $\omega_d=\gamma_d\sqrt{2V_d/m}$ is the angular frequency of oscillations at the bottom of $V_d(z)$]:

$$\phi_q(z)=\left[\frac{2}{L}\right]^{1/2}\Phi(\varepsilon,\xi-\xi_0) , \quad (2.24a)$$

$$\phi_n(z)=\sqrt{\gamma_0}\Phi_n(\xi-\xi_0) , \quad (2.24b)$$

$$\psi(z,t)=\sqrt{\gamma_0}f(\xi-\xi_0,\tau) . \quad (2.24c)$$

The functions $\Phi_n(\xi)$ and $\Phi(\varepsilon,\xi)$ along with the WKB form for the latter are listed in Appendix A. We note that the only parameter needed to specify the states of the physisorbed particle of mass m trapped in the potential $V_0(z)$ is $\sigma_0=\sqrt{2mV_0}/(\hbar\gamma_0)$. The function $f(\xi,\tau)$ is given in Appendix B. Besides σ_0, three other system parameters, $\mu=\gamma_0/\gamma_d$, $\beta=(V_0\gamma_0^2/V_d\gamma_d^2)^{1/2}=\omega_0/\omega_d$, and $s=\exp[-\gamma_d(z_0-z_d)]$, accounting, respectively, for the ratio of the widths of both potentials, the ratio of their low-energy oscillation frequencies, and the mismatch of their equilibrium positions, appear in it.

Combining the results (2.15), (2.18), (2.20), and (2.24a) and (2.24c), we obtain the following expression for the (dimensionless) kinetic-energy distribution of particles desorbing in the direction normal to the surface:

$$R(\varepsilon)\equiv\frac{\hbar\omega_L}{4}\left[\frac{d\dot{N}(E)}{dE}\right]=\frac{\varepsilon}{w}\int_0^\infty e^{-\tau/w}R(\varepsilon,\tau)d\tau , \quad (2.25)$$

where $w=\omega_d/\lambda$. Similarly, from Eqs. (2.16), (2.17), (2.24b), and (2.24c), we get two alternative expressions for the total desorption yield:

$$Y=1-\frac{1}{w}\sum_n\int_0^\infty e^{-\tau/w}R_n(\tau)d\tau=\int_0^\infty\varepsilon^{-1}R(\varepsilon)d\varepsilon . \quad (2.26)$$

The factor ε in front of the integral in Eq. (2.25) converts the one-dimensional distribution into the three-dimensional one, as seen in Eq. (2.20). It is canceled by ε^{-1} in the integrand of Eq. (2.26) because the total desorption yield is entirely determined by the one-dimensional theory. The integrands in Eqs. (2.25) and (2.26) are

$$R(\varepsilon,\tau)=\frac{\sigma_0}{\pi\sqrt{\varepsilon}}\left|\int_{-\infty}^\infty d\xi\,\Phi(\varepsilon,\xi)f(\xi,\tau)\right|^2 \quad (2.27)$$

and

$$R_n(\tau)=\frac{n!(2\sigma_0-2n-1)}{\Gamma(2\sigma_0-n)} \times\left|\int_{-\infty}^\infty d\xi\exp(-\sigma_0e^{-\xi})(2\sigma_0e^{-\xi})^{\sigma_0-n-1/2} \times L_n^{2\sigma_0-2n-1}(2\sigma_0e^{-\xi})f(\xi,\tau)\right|^2 . \quad (2.28)$$

The explicit form of $\Phi_n(\xi)$, Eq. (A1), was used in Eq. (2.28). $\Phi(\varepsilon,\xi)$ and $f(\xi,\tau)$ are given in Eqs. (A2), and (B2), respectively. In the particular case in which the equilibrium positions of both potentials coincide ($z_0=z_d$), the function $f(\xi,\tau)$ is a periodic function of time [cf. Eqs. (B2) and (B10)]. This periodicity can be used to transform the τ integration in Eqs. (2.25) and (2.26), which now reads

$$R(\varepsilon)=\varepsilon\int_0^{\pi/2}\frac{\cosh[(\tau-\pi/2)w]}{w\sinh(\pi/2w)}R(\varepsilon,\tau)d\tau \quad (2.29)$$

and

$$Y=1-\sum_n\int_0^{\pi/2}\frac{\cosh[(\tau-\pi/2)/w]}{w\sinh(\pi/2w)}R_n(\tau)d\tau , \quad (2.30)$$

respectively, allowing us, when $z_0=z_d$ to carry on the numerical calculations for larger values of w than in the general case of $z_0\neq z_d$.

D. Approximations and special cases

Any physical system to be considered within the model presented here is characterized by m, V_0, V_d, γ_0, γ_d, z_0, z_d, and λ being, respectively, the mass of the adsorbed particle, the depth, the range parameter, and the equilibrium position of each of the potentials, and the electronic deexcitation rate. They combine into five dimensionless parameters,

$$\sigma_0=\left[\frac{2mV_0}{\hbar^2\gamma_0^2}\right]^{1/2},\quad \beta=\left[\frac{V_0}{V_d}\right]^{1/2}\frac{\gamma_0}{\gamma_d}=\frac{\omega_0}{\omega_d},$$
$$\mu=\frac{\gamma_0}{\gamma_d},\quad s=e^{-\gamma_d(z_0-z_d)},\quad w=\frac{\omega_d}{\lambda}. \tag{2.31}$$

It is worthwhile at this stage to take a note of the physical meaning of these parameters. The first one, σ_0 is the usual strength parameter of the ground-state potential. The next three parameters express three parameters specifying the excited-state potential (V_d, γ_d, and z_d) in terms of the parameters of the ground-state potential. Thus, β is the ratio of the oscillation frequencies at the bottoms of both potentials. For $\beta<1$ the excited-state potential is, at its bottom, narrower than $V_0(z)$. The parameter μ measures the width of the excited-state potential and $\mu<1$ if the latter is globally narrower than $V_0(z)$. Finally, s is determined by the position of the minimum of the excited-state potential. For $s=1$ the equilibrium positions of both potentials coincide and for $s<1$ the excited-state potential binds the particle closer to the surface than $V_0(z)$ does. In all physically interesting situations all three parameters are smaller than 1. Note that the ratio of depths of both potentials is $V_d/V_0=(\mu/\beta)^2$. The last parameter w is proportional to the lifetime of the metastable excited state. For $w\approx 1$, the lifetime is of the order of the oscillation period at the bottom of $V_d(z)$.

Typical systems for which the kinetic-energy distributions were measured are N_2O,[10,11] and Ar, and Kr (Ref. 14) physisorbed on Ru(001) for which $V_0=430$, 109, and 162 meV, respectively. Little is known about the range parameter γ_0. Taking $\gamma_0=1$ Å^{-1}, one gets, respectively, $\sigma_0=95.48$, 45.8, and 80.6. Incidentally, the surface potential for Ar/Ru (001) calculated by Walkup *et al.*[29] using the local density functional (LDF) method has $V_0=65.7$ meV and $\gamma_0=0.792$ Å^{-1}, resulting in $\sigma_0=44.9$, almost the same value as the one given above for this system. The remaining parameters will be specified later on.

Desorption yields can be calculated from Eqs. (2.26) and (2.28) without any further approximations. However, calculation of the distribution $R(\varepsilon)$ is a very demanding numerical task because of rapid oscillations exhibited by the continuum wave function $\Phi(\varepsilon,\xi)$ and the fact that the Gaussian $f(\xi,\tau)$ becomes for some values of τ a quite sharply peaked function of ξ. This makes the calculation of $R(\varepsilon,\tau)$ numerically unstable and time consuming, particularly for the large values of σ_0 considered here, even if the WKB form (A5) or (A8) is used for the continuum wave functions.

However, a very simple algebraic approximation for $R(\varepsilon,\tau)$ can be obtained. This approximation not only results in manageable numerics but also allows us to gain additional insight into the obtained results. We discuss this approximation in some detail for the case of potentials with coincident minima ($s=1$; we can set $z_0=z_d\equiv 0$ in this case), but it can and will be also used in a more general case. The approximation is suggested by analyzing Fig. 1 in which both potentials, the continuum wave function $\Phi(\varepsilon=2,\xi)$, and the real part of the Gaussian wave packet (B2) [with $F(\tau)$ given by Eq. (B10)] for three values of τ between 0 and $\pi/2$ are plotted. The center of the time-dependent wave packet remains at $z=z_0=z_d=0$ and $V_d(z)$ can be represented by a parabola in Fig. 1 because only the curvature of this potential at its bottom (i.e., β but not μ) determines the time evolution of this wave packet [cf. Eq. (2.23)]. The wave packet has the largest width at $\tau=0$ and never penetrates regions close to the classical turning point in $V_0(z)$. In such a case, Fig. 1 suggests that $\Phi(\varepsilon,\xi)$ can be approximated by a simple sinusoidal standing wave,

$$\Phi(\varepsilon,\xi)=A(\varepsilon)\sin[\sigma_0\sqrt{\varepsilon+1}\,\xi+\delta(\varepsilon)]\ , \tag{2.32}$$

for all positions ξ for which the value of the Gaussian is significant. In Eq. (2.32) $\sigma_0\sqrt{\varepsilon+1}$ is the (dimensionless) de Broglie wave number of the particle at $\xi=\xi_0\equiv 0$. The amplitude $A(\varepsilon)$ and the phase shift $\delta(\varepsilon)$ can be determined by comparing the above form with the WKB approximation (A8). This is done in Appendix C [cf. Eqs. (C2)–(C4)]. The form (2.32) might be termed SWKB, standing for a simplistic WKB approximation. The integral in Eq. (2.27) can be now calculated analytically and the result is proportional to $\Phi(\varepsilon,\xi=0)$. Inserting this re-

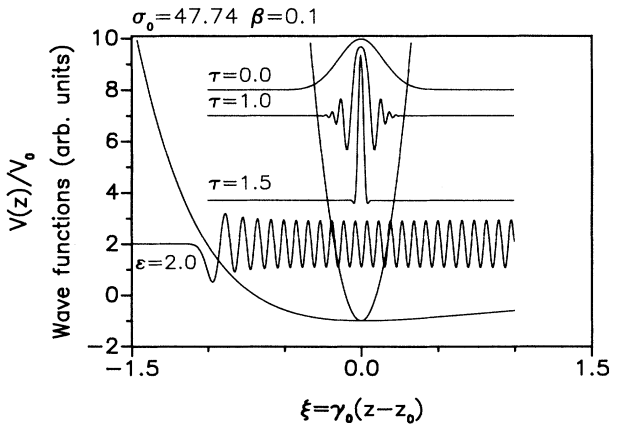

FIG. 1. Surface potentials $V_0(z)$ and $V_d(z)$, continuum wave function $\Phi(\varepsilon,\xi)$ [Eq. (A2)] for $\varepsilon=2.0$, and real parts of Gaussian wave packets $f(\xi,\tau)$ [Eq. (B2)] for $\tau=0$, 1.0, and 1.5 for the case $z_0=z_d$. For this case only the curvature of $V_d(z)$ at its bottom affects the time evolution of the wave packets so this potential is represented by a parabola. The wave functions and wave packets are displaced vertically in order to avoid their overlapping.

sult into Eq. (2.25) together with $\Phi(\varepsilon,\xi=0)$ obtained from Eq. (A8), we get

$$R(\varepsilon)=\sin^2\left[\sigma_0\left[\sqrt{\varepsilon}\sinh^{-1}(\sqrt{\varepsilon})-\sqrt{\varepsilon+1}+\frac{\pi}{2}\right]+\frac{\pi}{4}\right]$$
$$\times\frac{2\varepsilon}{\sqrt{\pi(\varepsilon+1)}}\int_0^{\pi/2}d\tau\frac{\cosh[(\tau-\pi/2)/w]}{w\sinh(\pi/2w)}$$
$$\times[\sigma_0F_R(\tau)]^{1/2}\exp[-(\varepsilon+1)\sigma_0F_R(\tau)]\ , \qquad (2.33)$$

where

$$F_R(\tau)\equiv\frac{F_r(\tau)}{|F(\tau)|^2}=\beta^2\frac{1+\tan^2\tau}{\beta^2+\tan^2\tau} \qquad (2.34)$$

for $s=1$ [cf. Eq. (B10)]. Similar results are obtained for $z_0\neq z_d$ ($s\neq1$) but the result is a bit lengthy and we quote it in Appendix C, Eq. (C5).

Anticipating the discussion in Sec. III, we note that for our numerical work the SWKB approximation (2.33) and/or (C5) is used unless stated otherwise. This approximation becomes unreliable for (i) very small values of σ_0 because then the continuum spectrum wave function cannot be approximated in any ξ interval by a sinusoidal standing wave. It also fails when (ii) a significant part of the time-dependent wave packet $\psi(z,t)$ penetrates regions close to or beyond the classical inner turning point in $V_0(z)$. This may happen for a certain choice of system parameters—for example, when the theory is applied to the standard Antoniewicz situation and $V_d(z)$ is very wide. In such cases more numerically involved calculations employing Eqs. (2.25), (2.27), (A5), and (B2) are necessary. Such calculations were also occasionally done to verify the accuracy of the SWKB approximation in cases in which it was used.

We pause to discuss few features of the result (2.23) obtained for $z_0=z_d$. The energy distribution $R(\varepsilon)$ factors out into a product of the ε-dependent time integral times the square of the continuum wave function $\Phi(\varepsilon,\xi=0)$ taken at the position of the center of the wave packet, i.e., at the equilibrium position of both potentials. The continuum wave function is a standing wave resulting from the interference of the incoming and reflected waves with positions of its nodes depending on ε. One thus expects that the energy distribution $R(\varepsilon)$ will exhibit, as a function of ε, quite rapid oscillations as the nodes and the antinodes pass through $\xi=\xi_0\equiv0$: No particles are desorbed at energies corresponding to the Ramsauer-Townsend resonances at $\xi=0$. These oscillations are contained in the $\sin^2(\cdots)$ factor in Eq. (2.33). The spacing between the resonances (i.e., the period of the oscillations) is inversely proportional to σ_0 (it is roughly equal to $2\pi/\sigma_0$) and increases slowly with increasing energy. When the equilibrium positions of both potentials are somewhat mismatched ($z_d<z_0$, i.e., $s<1$; cf. Appendix C), the position of the center of the wave packet depends on time τ and the integration (2.27) results in $R(\varepsilon,\tau)$, which again is an oscillatory function of ε. The explicit form of $R(\varepsilon,\tau)$ in this case in SWKB approximation can be easily extracted from Eq. (C5) by comparing it with Eq. (2.25). The oscillation period and the phase of $R(\varepsilon,\tau)$ depend now on τ so that the oscillating term cannot be pulled outside of the time integral in Eq. (2.25) as seen in Eq. (C5). The amplitude of the oscillations of the resulting distribution $R(\varepsilon)$ is now diminished due to the smoothing-out effect of the time integration. For smaller values of σ_0 and/or s close to 1, the smoothing out is not complete. For larger σ_0 and/or significantly mismatched equilibrium positions of both potentials, the oscillations of $R(\varepsilon)$ may be, and indeed are, entirely washed out.

Returning to the case of $z_0=z_d$, we note that the entire factor in the second line of Eq. (2.33) forms a slowly varying envelope on which the oscillations just discussed are superimposed. The envelope function increases linearly for small ε, reaches a maximum, and then decreases roughly exponentially. It is interesting to note that the dominant dependence on the parameters σ_0 and β in the envelope is through the product $p=\sigma_0\beta^2$. The additional dependence on β in the denominator of F_R is much less important for $\beta^2\ll1$. Instead of calculating the desorption yield from Eq. (2.30), one can estimate it averaging $R(\varepsilon)$ over the oscillations by replacing the $\sin^2(\cdots)$ factor in Eq. (2.33) by its average value of 0.5 and integrating the result over ε according to the right-hand side of Eq. (2.26). The result is

$$Y\approx\int_0^{\pi/2}d\tau\frac{\cosh[(\tau-\pi/2)/w]}{w\sin(\pi/2w)}\mathrm{erfc}[\sqrt{\sigma_0F_R(\tau)}]\ , \qquad (2.35)$$

where erfc is a complementary error function.[30]

III. NUMERICAL RESULTS

A. Flexibility of the model and comparison with earlier calculations

We start our analysis of the numerical results by presenting in Fig. 2 typical kinetic-energy distributions obtained for some model potentials. All distributions

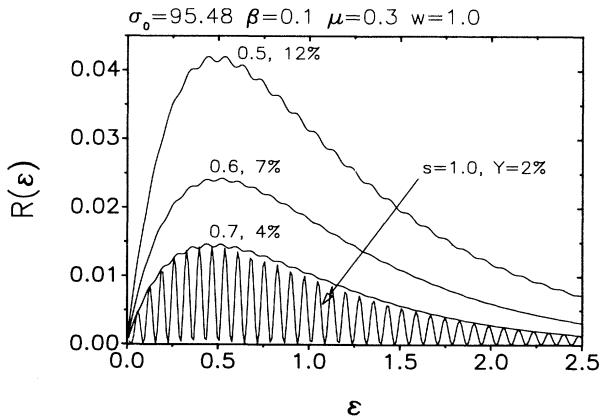

FIG. 2. Typical kinetic-energy distributions obtained in the present model for various values of z_0-z_d. Dimensionless parameters are listed at the top of the figure. Numbers beside the curves are the values of $s=\exp[-\gamma_d(z_0-z_d)]$ and of the overall desorption yield Y.

were calculated using SWKB approximation, i.e., Eq. (C5) for $s \neq 1.0$ and Eq. (2.33) for $s=1.0$. For $\beta < 1.0$, potential $V_d(z)$ is narrower at its bottom than $V_0(z)$ and for the particular parameters chosen it is $(\mu/\beta)^2 = 5.6$ times deeper than the latter. For $s=1.0$, equilibrium positions of both potentials coincide and, as expected, the resulting distribution exhibits strong Ramsauer-Townsend oscillations as a function of ε. For $s < 1.0$, the equilibrium position of $V_d(z)$ is closer to the surface than that of $V_0(z)$ (i.e., $z_d < z_0$), but the shift is small enough for the SWKB approximation to be still valid. Indeed, it was checked that the results obtained without SWKB using Eqs. (2.25), (2.27), (A5), and (B2) cannot be distinguished within the accuracy of the graph from those in Fig. 2. We note that even for a small mismatch of the equilibrium positions of both potentials ($s \approx 1$) the amplitude of the Ramsauer-Townsend oscillations is drastically reduced. The absolute desorption yield increases from 2% for $s=1.0$ up to 12% for $s=0.5$, whereas the position of the maximum of the distribution is weakly affected by s. Additional calculations for other sets of parameters reveal that, in general, the energy at which the distribution peaks increases with decreasing s and/or with increasing μ. The distributions in Fig. 2 are for $w=1.0$, i.e., the lifetime of A^* is of the order of the oscillation period $2\pi/\omega_d$ at the bottom of $V_d(z)$. Increasing the lifetime above $w=1.0$ does not change the shape of the distributions and leads to an increase of the overall desorption yields by a factor not larger than 1.5 above those in Fig. 2 (of course, the yield tends to zero the limit $w \to 0$). This feature is in a sharp contrast to the results obtained in the standard Antoniewicz model in which the increase of the lifetime substantially increases desorption yields and shifts distribution maxima towards higher energies.[15,16] For $s=1.0$ ($z_0 = z_d$), the results do not depend on μ [cf. Eq. (2.33)] and the oscillation period seen in Fig. 2 is roughly equal to $2\pi/\sigma_0$. Therefore, smoothing out the oscillations by decreasing s is less effective for smaller σ_0 than it is for larger ones. It was checked that for $\sigma_0 = 120$ the Ramsauer-Townsend oscillations totally disappear for s as close to unity as 0.8.

There is not *a priori* any limitation on widths, depths, and equilibrium positions of both potentials which can be used in the present model. Therefore, the model contains the standard Antoniewicz desorption scenario (with the position-independent reneutralization rate λ) as a particular case. We can, therefore, test the adequacy of the Gaussian wave-packet approach by applying the present model to cases previously studied in Refs. 15 and 16. In these papers the classical and exact quantum-mechanical approach to the Antoniewicz model using Morse potentials for both $V_0(z)$ and the image potential $V_d(z)$ was developed. Analytical, numerically manageable results of the exact quantum-mechanical approach could be obtained only for $\gamma_d = \gamma_0$ (i.e., $\mu=1$) and $\beta=s$.[15,16] This was not a serious restriction for the *Antoniewicz* model because the time-dependent wave packet has just enough time (before the reneutralization occurs) to probe the potential $V_d(z)$ only in the immediate vicinity of $z=z_0$. Thus, beside σ_0 and w, the only other system parameter in this version of the Antoniewicz model is the slope of $V_d(z)$ at the initial position $z=z_0$. Other details of $V_d(z)$ are irrelevant. The requirement that this slope be equal to the slope of the Coulomb image potential at the same point fixes the value of β (and of s). We compare now the results of the present approach applied to the Antoniewicz model with the results of Refs. 15 and 16 using exactly the same system parameters as theirs. Naturally, such a comparison can only be done for the position-independent deexcitation rate λ.

In Fig. 3 the kinetic-energy distributions of desorbing neutral N_2O molecules physisorbed on Ru(001) are shown, calculated using the classical and the exact quantum-mechanical versions of the Antoniewicz model,[15,16] and the present approximate quantum-mechanical approach. The parameters used are those of Ref. 15 and 16. We note that the results of the exact quantum-mechanical approach (dotted curve) and these of the present one without SWKB approximation (solid curve) are for all practical purposes identical, whereas use of the SWKB approximation (short dashes) results in yields that are too low, although the latter results are also not too far off the mark. This inadequacy of SWKB in the present case is not surprising because for the potentials used in this calculation a substantial portion of the time-dependent wave packet can penetrate regions close to and beyond the classical turning point

$$[\gamma_0(z-z_0) = -\ln(1+\sqrt{1+\varepsilon})]$$

of $V_0(z)$ for almost all energies ε of interest. We note

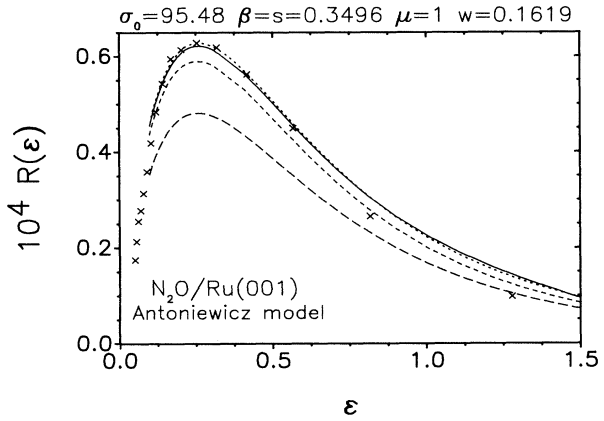

FIG. 3. Kinetic-energy distributions of desorbing N_2O molecules from Ru(001) surface in the Antoniewicz model (with position-independent neutralization rate) obtained using different approximations: exact quantum theory of Refs. 15 and 16 (dotted curve); present approach without SWKB approximation (solid curve); present approach with SWKB approximation (short dashes); classical theory of Refs. 15 and 16 (long dashes). Experimental results (normalized to match the exact quantum-mechanical distribution at the maximum) are also shown. Parameters (the same as in Refs. 15 and 16): $V_0 = 430$ meV, $\gamma_0 = 1$, Å^{-1}, $z_0 - z_{im} + 1.5$ Å (z_m is the position of the image plane), and $\lambda = 2.4 \times 10^{14}\ \text{s}^{-1}$, resulting in the dimensionless parameters listed above the figure. The overall calculated desorption yield $\approx 10^{-3}\%$ is about 3 orders of magnitude lower than observed experimentally.

also that the classical approach results in the distribution (long dashes), which becomes indistinguishable from the exact quantum-mechanical one (dotted) after both are normalized to a common value at their maximum. Experimental results are also shown in Fig. 3. We point out, however, that although the shape of the theoretical distribution matches quite well the experimental one, the calculated overall desorption yield is three orders of magnitude too low (for a detailed discussion of this point, see Refs. 15, 16, and 21).

Results of a test similar to the above one done for He/W, another system theoretically investigated in Refs. 15 and 16, are shown in Fig. 4. Here, SWKB approximation entirely fails because for all interesting energies the center of the time-dependent wave packet penetrates into the classically forbidden region of $V_0(z)$ and also because σ_0 is very small. The results shown in Fig. 4 (solid curve) are thus obtained without employing SWKB approximation [i.e., WKB approximation (A5) along with Eqs. (2.25), (2.27), and (B2) are used]. We note gentle oscillations of the kinetic-energy distribution which for such a small value of σ_0 are not entirely washed out despite quite substantial mismatch of the equilibrium positions of both potentials (s much smaller than 1). Interestingly, the exact quantum-mechanical theory of Ref. 15 (dotted curve) not only does not show any of the Ramsauer-Townsend oscillations, but also predicts that the distribution peaks at energies much lower than those predicted by both the present model and the entirely classical approach (dashes). Indeed, as seen in Fig. 4, the latter two distributions peak at approximately the same energy, provided the Ramsauer-Townsend oscillations are ignored. There might be two possible reasons for the discrepancy of the results obtained in the exact quantum and in the present approximate quantum-mechanical approach: (i) One can argue that the Gaussian approach, being quasiclassical in nature, should result in predictions closer to the classical than to the exact quantum-mechanical ones. Such an explanation remains on rather shaky ground: For N_2O/Ru(001) discussed above, just the opposite happens. We are rather encouraged to believe that (ii) the exact quantum-mechanical approach of Ref. 15 is faulty for the He/W system because of the following reason. In the exact quantum-mechanical approach a tacit assumption is made[15] that wave functions of the bound states $V_d(z)$ form a basis complete enough to expand faithfully the time-dependent wave packet $\psi(z,t)$. Continuum-state wave functions are never included in this set. This approximation works perfectly for a majority of the cases. For example, for N_2O/Ru(001) this (bound-states-only) basis contains 270 functions[15,16] but about 150 of them, corresponding to the lowest bound states, suffice to obtain the accurate results. For He/W the corresponding number is 134, but leaving out even few of them alters the results substantially, indicating that the basis should probably also contain the continuum spectrum of $V_d(z)$.

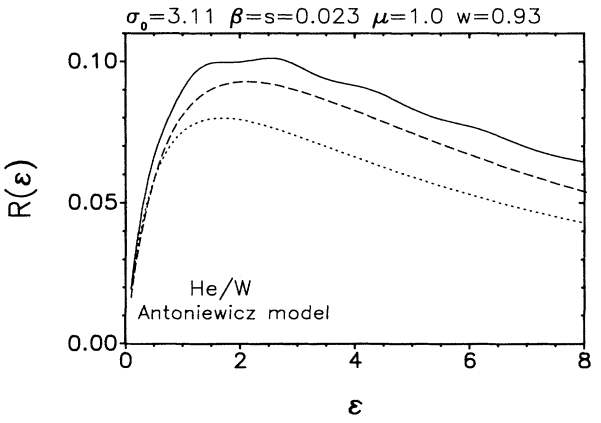

FIG. 4. Same as Fig. 3, but for He/W system: exact quantum theory (dotted curve); present approach without SWKB approximation (solid curve); classical theory (long dashes). Parameters (the same as in Refs. 15 and 16): $V_0=5.23$ meV, $\gamma_0=1$ Å^{-1}, $z_0-z_{im}+2.83$ Å, and $\lambda=2.4\times10^{14}$ s^{-1}, resulting in the dimensionless parameters listed above the figure.

B. Application to Ar and N_2O on Ru(001)

As mentioned already in the Introduction, the standard Antoniewicz model fails when confronted with the experimental data. Therefore, we want to apply the model considered in this paper to ESD of N_2O and Ar from Ru(001). The results of this section were already reported.[24]

The only relatively well-established parameter is the binding energy of the physisorbed particles to the monolayer covered surface: 109 and 430 meV for Ar (Ref. 14) and N_2O (Ref. 15), respectively. Consequently, these values for V_0 [cf. Eq. (2.21a)] were used in *all* calculations. The parameter γ_0 is far less certain so we have decided to do our tests for $\gamma_0=1.0$ and 0.5 Å^{-1}. The parameters z_0 and z_d enter the theory only through the difference z_0-z_d present in s. Adopting the view that $V_d(z)$ binds the adsorbed particle stronger and closer to the surface than $V_0(z)$ does, we have set the restrictions $z_0-z_d>0$, $V_d>V_0$, and $\gamma_d>\gamma_0$ on the parameters of $V_d(z)$, but did not try to restrict them otherwise. In terms of the dimensionless parameters defined in Eq. (2.31), these restrictions read $\beta<1$, $\mu<1$, and $s\leq1$. Finally, the electronic deexcitation rate λ was chosen to be of the order of 10^{13} s^{-1} implying w of the order of 1.

The representative fits for $\gamma_0=1.0$ Å^{-1} resulting in the highest yield we were able to obtain are given in Figs. 5 and 6 for Ar and N_2O, respectively. The potentials used to obtain these particular fits are plotted in Fig. 7, and the dimensionless parameters (2.31) are listed in respective figure captions. The experimentally determined yields are known with a substantial uncertainty: They are estimated to be less than some 10% for N_2O and about 60% for Ar although the arguments were forwarded[17] that the value of 20% would not be unrealistic in the latter case. Our theoretical yields are certainly lower: 0.83% and 24% for N_2O and Ar, respectively. However, they represent a remarkable improvement over *the best* results the Antoniewicz model was ever capable of: 0.005–0.01 % for N_2O (Refs. 15 and 16) and 1–3 % for

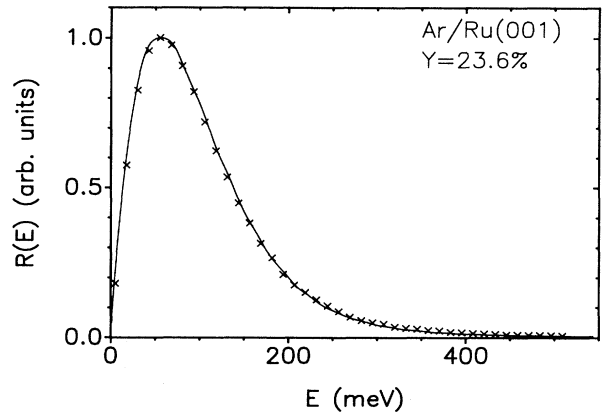

FIG. 5. Theoretical (solid curve) and experimental (crosses) results for the kinetic-energy distribution of Ar atoms desorbing from a monolayer physisorbed on Ru(001). Parameters used: $V_0=109$ meV, $\gamma_0=1$ Å^{-1}, $V_d=857$ meV, $\gamma_d=1.43$ Å^{-1}, $z_0-z_d=0.32$ Å, $\lambda=0.97\times10^{13}$ s^{-1}, resulting in the dimensionless parameters $\sigma_0=45.8$, $\beta=0.25$, $\mu=0.7$, $s=0.63$, $w=3.0$. Both distributions are normalized to 1 at their maximum.

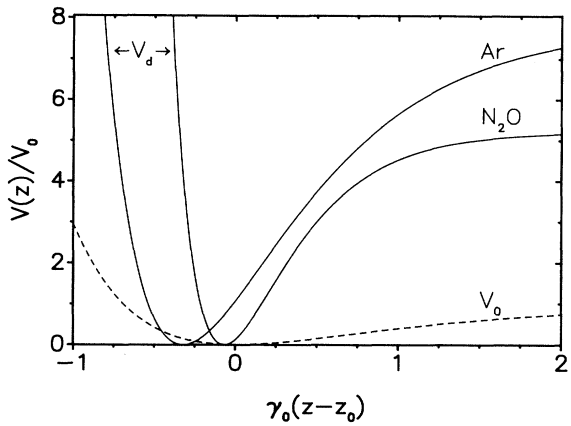

FIG. 7. Morse potentials $V_0(z)$ and $V_d(z)$ used in the calculations presented in Figs. 5 and 6. In dimensionless variables adopted here $V_0(z)$ is represented by the same curve for both systems.

for Ar.[21] The higher values quoted here were obtained assuming rather unrealistically strong position dependence of the reneutralization rate λ. In our present approach λ is constant. Further improvement is expected once λ's position dependence is accounted for.

For almost all best fits (including those for which we have used $\gamma_0=0.5$ Å^{-1}, not shown here) we have obtained for both systems, the value of z_0-z_a is between 0.3 and 0.4 Å for Ar and between 0.06 and 0.12 Å for N_2O. The ratio $\mu=\gamma_0/\gamma_d$ stays between 0.5 and 0.7 for Ar and between 0.2 and 0.4 for N_2O. Once the value of γ_0 was chosen (0.5 or 1.0 Å^{-1}), then the shape of the distribution determines the ratio of frequencies at the bottom of both potentials $\beta=\omega_0/\omega_d$, uniquely. As discussed in Sec. III A, the overall shape of the theoretical distributions (i.e., the position of the maximum and the high energy tail) is quite insensitive to λ (i.e., insensitive to w). Also, the total yield, although initially becoming larger for longer lifetime (smaller λ), does not increase any more once λ^{-1} becomes equal to or larger than about half of the oscillation period at the bottom of $V_d(z)$ (about 10^{-14} s for both systems) i.e., once w becomes equal or somewhat larger than 2. For comparison, even small variations of λ in the Antoniewicz case (again around 10^{-14}–10^{13} s) drastically affect the shape of the distributions and yields. We also note that the kinetic-energy distribution for N_2O exhibits remnants of the Ramsauer-Townsend oscillations while they are almost absent in the distributions for Ar. Responsible for this difference is the quite different mismatch of the equilibrium positions of $V_0(z)$ and $V_d(z)$ in these two cases, as seen in Fig. 7, which nullifies the effect of smaller σ_0 for Ar.

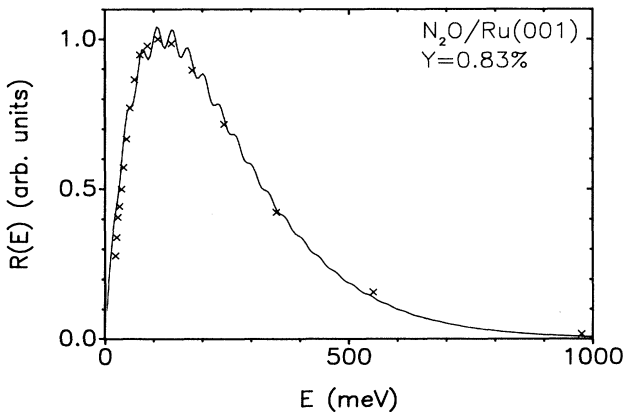

FIG. 6. Same as Fig. 5, but for N_2O physisorbed on Ru(001). Parameters used: $V_0=430$ meV, $\gamma_0=1$ Å^{-1}, $V_d=2.26$ eV, $\gamma_d=2.5$ Å^{-1}, $z_0-z_d=0.07$ Å, $\lambda=3.9\times10^{13}$ s^{-1}, resulting in the dimensionless parameters $\sigma_0=95.48$, $\beta=0.175$, $\mu=0.4$, $s=0.84$, $w=2.0$.

Before concluding, we must mention here the attempt by Hübner and Bennemann,[19] who, using the Antoniewicz model, could obtain a reasonable shape of the energy distribution and the yield approaching 60% for Ar/Ru(001). To do this, they were forced to assume a steplike position dependence of $\lambda=\lambda(z)$, which is difficult to justify physically. An interesting analysis of such a possibility was also given by Gortel and Tsukada.[28] On the other hand, Walkup *et al.*[17] were able to fit the distributions for the same system and obtain the yields of the order of 11% using the Antoniewicz model with both potentials calculated using the local density functional method. However, their high yield is a direct result of taking $V_0=65.7$ meV (Ref. 29) instead of the experimentally determined 109 meV. It happens because the theory predicts a sharp increase of the yield with increasing (dimensionless) kinetic energy $\varepsilon_{max}=E_{max}/V_0$ at which the *theoretical* distribution has a maximum. The *experimental* distributions peak around 56 meV. With $V_0=109$ meV, the system parameters must be chosen such that the *theoretical* distribution peaks at $\varepsilon_{max}=0.51$, whereas

for $V_0=67.5$ meV, the corresponding value is $\varepsilon_{max}=0.83$. Not surprisingly, the latter corresponds to higher yield. Using $V_0=67.5$ meV, we were able to reproduce the experimental distributions and get the yield as high as 15% using the standard Antoniewicz model and assuming a position dependence of λ much weaker than that which Walkup *et al.*[17] had to use. With $V_0=67.5$ meV our model would certainly predict the yields close to the experimental value of 61%. We feel, however, that the experimentally determined 109 meV is better justified and should be used in all calculations instead of the LDF value of 67.5 meV. The latter is probably appropriate for an isolated Ar atom physisorbed on a perfect Ru surface but the experiments are done at coverages close to a monolayer. Even at much lower coverages, desorption proceeds from islands where the binding energy is again closer to 109 meV (Ref. 31) and for such V_0 the Antoniewicz model cannot predict yields higher than about 3%.[21]

IV. FINAL COMMENTS AND CONCLUSIONS

We have proposed in this work a new model for electron-stimulated desorption of species physisorbed on solid surfaces. In contrast to the standard Antoniewicz model, we assume that the initial electronic excitation of the system leads to a chemical bond with its equilibrium distance from the surface not far away from that for the Van der Waals surface potential. Some indication that such is the nature of the excited-state potential follows from the cluster calculations of Jennison *et al.*[22] but more work is needed to identify this state uniquely. The necessary desorption increase of the kinetic energy of the particle evolving on the excited-state potential energy surface is achieved due to the increase of the momentum uncertainty of a squeezed wave packet. Therefore, desorption is a purely quantum-mechanical effect unlike in the Antoniewicz model in which a classical theory suffices. A remarkable consistency between the experimental data and the predictions of the model, was obtained for all systems for which accurate experimental results exist: both the overall desorption yield and the shape of the kinetic-energy distributions of desorbing neutrals are correctly accounted for. We predict and discuss the origin of oscillations which may occur on the kinetic-energy distribution curves. In this paper we give also a microscopic justification of one-dimensional models used usually to describe the electron-stimulated desorption. To our knowledge, no such justification was ever attempted. The present formulation allows generalizations to real three-dimensional models to be done and also allows us to calculate the angular distributions in ESD (ESDAD). Work on ESDAD is now in progress.

ACKNOWLEDGMENTS

This work has been supported by an operating grant from the Natural Sciences and Engineering Research Council of Canada.

APPENDIX A

Bound-state energies of a particle moving in the Morse potential $V_0(z)$ given in Eq. (2.21a) are equal to

$$\mathcal{E}_n=-V_0[(\sigma_0-n-\tfrac{1}{2})/\sigma_0]^2 ,$$

for

$$n=0,1,2,\ldots,n_{max}\le\sigma_0-\tfrac{1}{2} ,$$

where $\sigma_0=\sqrt{2mV_0}/(\hbar\gamma_0)$. The corresponding wave functions can be written as

$$\phi_n(z)=\sqrt{\gamma_0}\Phi_n(\xi-\xi_0) ,$$

where $\xi=\gamma_0 z$, $\xi_0=\gamma_0 z_0$ are dimensionless positions, and

$$\Phi_n(\xi)=\left[\frac{n!(2\sigma_0-2n-1)}{\Gamma(2\sigma_0-n)}\right]^{1/2}\exp(-\sigma_0 e^{-\xi})\times(2\sigma_0 e^{-\xi})^{\sigma_0-n-1/2}L_n^{2\sigma_0-2n-1}(2\sigma_0 e^{-\xi}) . \quad (A1)$$

$\Gamma(x)$ and $L_n^{\alpha}(x)$ are, respectively, Euler's γ function and the generalized Laguerre polynomial of degree n.[30]

The wave functions for the continuum spectrum can be written as

$$\phi_q(z)=\sqrt{2/L}\,\Phi(\varepsilon,\xi-\xi_0) ,$$

where $\varepsilon=(\hbar q)^2/2mV_0$ and

$$\Phi(\varepsilon,\xi)=\left|\frac{\Gamma(\frac{1}{2}-\sigma_0-i\sigma_0\sqrt{\varepsilon})}{2\Gamma(2i\sigma_0\sqrt{\varepsilon})}\right|(2\sigma_0 e^{-\xi})^{-1/2}\times W_{\sigma_0,i\sigma_0\sqrt{\varepsilon}}(2\sigma_0 e^{-\xi}) , \quad (A2)$$

with $W_{\kappa,\mu}(x)$ being the Whittaker function.[30] The above form, although very useful for analytical calculations, is numerically unstable for σ_0 larger than about 20 (or somewhat higher depending on the computer used). In such cases it is more convenient to find $\Phi(\varepsilon,\xi)$, integrating numerically the (dimensionless) Schrödinger equation

$$\left[\frac{d^2}{d\xi^2}+\sigma_0^2[\varepsilon-e^{-\xi}(e^{-\xi}-2)]\right]\Phi(\varepsilon,\xi)=0 , \quad (A3)$$

with the boundary condition

$$\lim_{\xi\to\infty}\Phi(\varepsilon,\xi)=\cos\left[\sigma_0\sqrt{\varepsilon}[\xi-\ln(2\sigma_0)]-\arg\left[\frac{\Gamma(-2i\sigma_0\sqrt{\varepsilon})}{\Gamma(\frac{1}{2}-\sigma_0-i\sigma_0\sqrt{\varepsilon})}\right]\right] . \quad (A4)$$

The decay of $\Phi(\varepsilon,\xi)$ for negative ξ is so rapid that the numerical integration can be started assuming that $\Phi=0$ at ξ of the order of -2.0. However, for all cases of interest the WKB form is an excellent approximation to $\Phi(\varepsilon,\xi)$. It allows not only for faster numerical calculations but it also can be a starting point for further approximations used in this work. For the Morse potential it reads[32]

$$\Phi(\varepsilon,\xi)=\left[\pi^2\varepsilon\left|\frac{g(\xi)}{\varepsilon+2x-x^2}\right|\right]^{1/4}Ai[-g(\xi)]\ , \quad \text{(A5)}$$

where $x=\exp(-\xi)$, $Ai(z)$ is the Airy function,[30] and $g(\xi)$ is given by

$$\begin{aligned} g(\xi)\equiv g_{(+)}(\xi) &= \left\{\tfrac{3}{2}\sigma_0\left[\sqrt{\varepsilon}\ln\left[\frac{x+\varepsilon+\sqrt{\varepsilon(\varepsilon+2x-x^2)}}{x\sqrt{\varepsilon+1}}\right]\right.\right. \\ &\quad +\cos^{-1}\left[\frac{x-1}{\sqrt{\varepsilon+1}}\right] \\ &\quad \left.\left.-\sqrt{\varepsilon+2x-x^2}\right]\right\}^{2/3}, \end{aligned} \quad \text{(A6)}$$

in the classically permitted region to the right of the classical turning point $[\xi>-\ln(1+\sqrt{1+\varepsilon})]$, and by

$$\begin{aligned} g(\xi)\equiv g_{(-)}(\xi) &= -\left\{-\tfrac{3}{2}\sigma_0\left[\ln\left[\frac{x-1+\sqrt{x^2-2x-\varepsilon}}{\sqrt{\varepsilon+1}}\right]\right.\right. \\ &\quad +\sqrt{\varepsilon}\cos^{-1}\left[\frac{x+\varepsilon}{x\sqrt{\varepsilon+1}}\right] \\ &\quad \left.\left.-\sqrt{x^2-2x-\varepsilon}\right]\right\}^{2/3}, \end{aligned} \quad \text{(A7)}$$

in the classically forbidden region to the left of it $[\xi<-\ln(1+\sqrt{1+\varepsilon})]$. Due to the extreme steepness of the repulsive part of $V_0(z)$, the asymptotic form of the WKB function can be used in most cases. We need it only for $\xi>-\ln(1+\sqrt{1}+\varepsilon)$ in this work and it reads

$$\Phi(\varepsilon,\xi)=\left[\frac{\varepsilon}{\varepsilon+2x-x^2}\right]^{1/4}\sin\left[\tfrac{2}{3}[g_{(+)}(\xi)]^{3/2}+\frac{\pi}{4}\right]. \quad \text{(A8)}$$

APPENDIX B

At $t=0$ the wave function of A^* is just the ground-state wave function $\phi_0(z)$ in the surface potential $V_0(z)$. It is given by Eq. (A1) and in Heller's[23] method it is approximated by the harmonic-potential ground-state wave function:

$$\begin{aligned} &\psi(z,t=0) \\ &=\sqrt{\gamma_0}[\Gamma(2\sigma_0-1)]^{-1/2} \\ &\quad\times\exp(-\sigma_0 e^{-(\xi-\xi_0)})(2\sigma_0 e^{-(\xi-\xi_0)})^{\sigma_0-1/2} \\ &\approx\sqrt{\gamma_0}(\sigma_0/\pi)^{1/4}\exp[-\sigma_0(\xi-\xi_0)^2/2]\ , \end{aligned} \quad \text{(B1)}$$

with the dimensionless parameters and variables defined above Eq. (A1). For $t>0$ the wave packet has a form (2.22) in which $z(t)$ and $p(t)$ represent a classical motion in the potential $V_d(z)$ with the initial conditions $z(0)=z_0$ and $p(0)=0$. Introducing the dimensionless time $\tau=\omega_d t$, where $\omega_d=\gamma_d\sqrt{(2V_d/m)}$ is the angular oscillation frequency at the bottom of $V_d(z)$, it is convenient to write

$$\psi(z,t)=\sqrt{\gamma_0}f(\xi-\xi_0,\tau)\ .$$

The explicit form of $f(\xi,\tau)$ is

$$\begin{aligned} f(\xi,\tau)= &\left[\frac{\sigma_0}{\pi}F_r(\tau)\right]^{1/4} \\ &\times\exp\left[-\sigma_0\left[\tfrac{1}{2}F(\tau)[\xi-\Delta\xi(\tau)]^2\right.\right. \\ &\left.\left.-\frac{i}{\beta}\Delta\xi'(\tau)[\xi-\Delta\xi(\tau)]\right]\right], \end{aligned} \quad \text{(B2)}$$

in which the classical motion and the classical momentum are represented by

$$\begin{aligned} \Delta\xi(\tau)&\equiv\gamma_0[z(t)-z_0] \\ &=\mu\ln\left[\frac{1+(1-s)\cos[\sqrt{s(2-s)}\tau]}{2-s}\right] \end{aligned} \quad \text{(B3)}$$

and

$$\Delta\xi'(\tau)\equiv d\Delta\xi(\tau)/d\tau=(\gamma_0/m\omega_d)p(t)\ ,$$

respectively. Three system parameters [cf. Eq. (2.31)] appear here: $\mu=\gamma_0/\gamma_d$, $\beta=(\gamma_0/\gamma_d)\sqrt{V_0/V_d}=\omega_0/\omega_d$, and $s=\exp[-\gamma_d(z_0-z_d)]$ accounting, respectively, for the ratio of the widths of both potentials, the ratio of their low-energy oscillation frequencies ($\omega_0=\gamma_0\sqrt{2V_0/m}$), and the mismatch of their equilibrium positions. The dimensionless function $F(\tau)$ in Eq. (B2) is related to $\alpha(t)$ in Eq. (2.22) as follows:

$$F(\tau)\equiv F_r(\tau)+iF_i(\tau)=-i\left[\frac{2}{m\omega_0}\right]\alpha(t)\ . \quad \text{(B4)}$$

The differential equation (2.23) for $\alpha(t)$ has the following solution:[33]

$$\begin{aligned} \alpha(t)=&\tfrac{1}{2}\left[2\alpha_0\left[\frac{\partial p}{\partial p_0}\right]_{z_0}+\left[\frac{\partial p}{\partial z_0}\right]_{p_0}\right] \\ &\times\left[2\alpha_0\left[\frac{\partial z}{\partial p_0}\right]_{z_0}+\left[\frac{\partial z}{\partial z_0}\right]_{p_0}\right]^{-1}, \end{aligned} \quad \text{(B5)}$$

where $\alpha_0=\alpha(t=0)$ and $[z(z_0,p_0;t),\ p(z_0,p_0;t)]$ is a classical motion in $V_d(z)$ for general initial conditions (z_0,p_0). For the Morse potential $V_d(z)$ and $\alpha_0=im\omega_0/2$, we get

$$F(\tau)=N(\tau)/D(\tau)\ , \quad \text{(B6)}$$

where

$$N(\tau)=\frac{s(2-s)}{1+(1-s)C(\tau)}\left[1-s+C(\tau)+i\frac{s}{\beta(2-s)}\right.$$
$$\left.\times\left[\frac{S(\tau)}{\sqrt{s(2-s)}}[2s(2-s)-1-(1-s)^3C(\tau)]-\tau(1-s)^2[1-s+C(\tau)]\right]\right], \quad \text{(B7)}$$

$$D(\tau)=\frac{s}{2-s}\{(s-1)[(s-1)\sqrt{s(2-s)}\tau S(\tau)-2]+[2-s(2-s)]C(\tau)\}+i\beta\sqrt{s(2-s)}S(\tau), \quad \text{(B8)}$$

and

$$S(\tau)=\sin[\sqrt{s(2-s)}\tau],$$
$$C(\tau)=\cos[\sqrt{s(2-s)}\tau]. \quad \text{(B9)}$$

In a particular case when the equilibrium positions of both potentials coincide, $z_0=z_d$, we have $s=1$, so $\Delta\xi(\tau)=\Delta\xi'(\tau)\equiv 0$ in Eq. (B2) and

$$F(\tau)=\frac{\beta+i\tan\tau}{\beta(1+i\beta\tan\tau)}. \quad \text{(B10)}$$

Note that in this case $f(\xi,\tau)$ does not depend on μ; $\psi(z,t)$ is a periodic function of time (period equal to $2\pi/\omega_d$); and if $V_d(z)$ is narrower than $V_0(z)$ (i.e., if $\beta<1$), then the wave packet narrows down during the first quarter of the oscillation period. Such a case is illustrated in Fig. 1.

APPENDIX C

To get an approximate expression for $R(\varepsilon,\tau)$ for the case when $z_0\neq z_d$, we observe that the function $f(\xi,\tau)$ in Eq. (2.27) is a Gaussian (B2) strongly peaked around the classical position $\xi=\Delta\xi(\tau)$. We can, therefore, expand the argument of $\sin(\ldots)$ in Eq. (A8) in powers of $\xi-\Delta\xi(\tau)$, neglecting all terms beyond the linear one and keeping only the lowest-order term in the amplitude. The result (referred to as SWKB in Sec. II D) is

$$\Phi(\varepsilon,\xi)\approx A(\varepsilon,\tau)\sin\{\sigma_0\eta(\varepsilon,\tau)[\xi-\Delta\xi(\tau)]+\delta(\varepsilon,\tau)\}, \quad \text{(C1)}$$

where

$$\eta(\varepsilon,\tau)=\{\varepsilon+2\exp[-\Delta\xi(\tau)]-\exp[-2\Delta\xi(\tau)]\}^{1/2}, \quad \text{(C2)}$$

$$A(\varepsilon,\tau)=\left[\frac{\varepsilon}{\eta^2(\varepsilon,\tau)}\right]^{1/4}, \quad \text{(C3)}$$

and

$$\delta(\varepsilon,\tau)=\tfrac{2}{3}[g_{(+)}(\Delta\xi(\tau)]^{3/2}+\frac{\pi}{4}, \quad \text{(C4)}$$

with $g_{(+)}(\xi)$ defined in Eq. (A6). The form (2.32) is obtained setting $\Delta\xi(\tau)=0$. The integration in Eq. (2.27) can be done analytically. Inserting the result in Eq. (2.25), we obtain

$$R(\varepsilon)=\frac{2\varepsilon}{\sqrt{\pi}w}\int_0^\infty d\tau\, e^{-\tau/w}\frac{[\sigma_0F_R(\tau)]^{1/2}}{\eta(\varepsilon,\tau)}\exp(-\sigma_0\{\eta^2(\varepsilon,\tau)+[\Delta\xi'(\tau)/\beta]^2\}F_R(\tau))$$
$$\times\left[\sinh^2\left[\frac{\sigma_0}{\beta}\Delta\xi'(\tau)\eta(\varepsilon,\tau)F_R(\tau)+\delta(\varepsilon,\tau)\right]+\sin^2\left[\frac{\sigma_0}{\beta}\Delta\xi'(\tau)\eta(\varepsilon,\tau)F_I(\tau)\right]\right], \quad \text{(C5)}$$

where

$$F_R(\tau)=F_r(\tau)/|F(\tau)|^2,\quad F_I(\tau)=F_i(\tau)/|F(\tau)|^2. \quad \text{(C6)}$$

For $z_d=z_0$ we have $\Delta\xi(\tau)=\Delta\xi'(\tau)\equiv 0$, $\eta(\varepsilon,\tau)=\sqrt{\varepsilon+1}$, $F_R(\tau)$ assumes a simple analytical form (2.34) and Eq. (C5) reduces to the expression (2.33). We note that in Eq. (C5) a smooth funtion of ε [i.e., $\sinh(\cdots)$ term] is added to the oscillating one and both depend on τ. Therefore, the oscillations of $R(\varepsilon)$ present in the case of potentials with coincident equilibrium positions get somewhat washed out in the general case.

[1]*Desorption Induced by Electronic Transitions, DIET I,* Vol. 24 of *Springer Series in Chemical Physics,* edited by N. H. Tolk, M. M. Traum, J. C. Tully, and D. Madey (Springer-Verlag, Berlin, 1983); *Desorption Induced by Electronic Transitions, DIET II,* Vol. 4 of *Springer Series in Surface Sciences,* edited by W. Brenig and D. Menzel (Springer-Verlag, Berlin, 1985); *Desorption Induced by Electronic Transitions, DIET III,* Vol. 13 of *Springer Series in Surface Sciences,* edited by R. H. Stulen and M. L. Knotek (Springer-Verlag, Berlin, 1988); *Desorption Induced by Electronic Transitions, DIET IV,* Vol. 19 of *Springer Series in Surface Sciences,* edited by G. Betz and P. Varga (Springer-Verlag, Berlin, 1990).

[2]P. Avouris and R. Walkup, Annu. Rev. Phys. Chem. **40**, 173 (1989).
[3]D. Menzel and R. Gomer, J. Chem. Phys. **41**, 3311 (1964).
[4]P. A. Redhead, Can. J. Phys. **42**, 886 (1964).
[5]P. R. Antoniewicz, Phys. Rev. B **21**, 3811 (1981).
[6]J. C. Tully, in *Desorption Induced by Electronic Transitions, DIET I,* Ref. 1, p. 31.
[7]Q. J. Zhang and R. Gomer, Surf. Sci. **109**, 587 (1981).
[8]Q. J. Zhang, R. Gomer, and D. R. Bowman, Surf. Sci. **129**, 535 (1983).
[9]E. R. Moog, J. Unguris, and M. B. Webb, Surf. Sci. **134**, 849 (1983).
[10]P. Feulner, W. Riedl, and D. Menzel, Phys. Rev. Lett. **50**, 986 (1983).
[11]P. Feulner, D. Menzel, H. J. Kreuzer, and Z. W. Gortel, Phys. Rev. Lett. **53**, 671 (1984).
[12]P. Feulner, in *Desorption Induced by Electronic Transitions, DIET II,* Ref. 1, p. 142.
[13]P. Feulner, S. Auer, T. Müller, A. Puschmann, and D. Menzel, in *Desorption Induced by Electronic Transitions, DIET III,* Ref. 1, p. 58.
[14]E. Steinacker and P. Feulner, Phys. Rev. B **40**, 11348 (1989).
[15]Z. W. Gortel, H. J. Kreuzer, P. Feulner, and D. Menzel, Phys. Rev. B **35**, 8951 (1987).
[16]Z. W. Gortel, R. Teshima, and H. J. Kreuzer, Phys. Rev. B **37**, 3183 (1988).
[17]R. E. Walkup, P. Avouris, N. D. Lang, and R. Kawai, Phys. Rev. Lett. **63**, 1972 (1989).
[18]W. Hübner and W. Brenig, Z. Phys. B **74**, 361 (1989).
[19]W. Hübner and K.-H. Bennemann, Z. Phys. B **78**, 131 (1990).
[20]J. W. Gadzuk and C. W. Clark, J. Chem. Phys. **91**, 3175 (1989).
[21]Z. W. Gortel, Surf. Sci. **231**, 193 (1990).
[22]D. R. Jennison, E. B. Stechel, and A. R. Burns, in *Desorption Induced by Electronic Transitions, DIET III,* Ref. 1, p. 167.
[23]E. J. Heller, J. Chem. Phys. **62**, 1544 (1975).
[24]Z. W. Gortel and A. Wierzbicki, Surf. Sci. Lett. **239**, L565 (1990).
[25]W. Brenig, Z. Phys. B **23**, 361 (1976).
[26]P. Schuck and W. Brenig, Z. Phys. B **46**, 137 (1982).
[27]W. Brenig, J. Phys. Soc. Jpn. **51**, 1914 (1982).
[28]Z. W. Gortel and M. Tsukada, Phys. Rev. B **39**, 11259 (1989).
[29]Reference 17 and D. Menzel (personal communication).
[30]*Handbook of Mathematical Functions,* Natl. Bur. Stand. Appl. Math. Ser. No. 55, edited by M. Abramowitz and I. A. Stegun (U.S. GPO, Washington, 1965).
[31]One of us (Z.W.G) is indebted to Professor D. Menzel for clarifying this point.
[32]B. H. Bransden and C. J. Joachain, *Introduction to Quantum Mechanics* (Longmans London, 1989).
[33]S.-Y. Lee and E. J. Heller, J. Chem. Phys. **76**, 3035 (1982).